Adipocyte-specific deletion of zinc finger protein 407 results in lipodystrophy and insulin resistance in mice

Alyssa Charrier [1,2], Xuan Xu [2], Bo-Jhih Guan, Justine Ngo, Anthony Wynshaw-Boris, Maria Hatzoglou, David A. Buchner [*]

Department of Genetics and Genome Sciences, Case Western Reserve University School of Medicine, Cleveland, OH, 44106, USA

ARTICLE INFO

ABSTRACT

PPARγ deficiency in humans and model organisms impairs the transcriptional control of adipogenesis and mature adipocyte function resulting in lipodystrophy and insulin resistance. Zinc finger protein 407 (ZFP407) positively regulates PPARγ target gene expression and insulin-stimulated glucose uptake in cultured adipocytes. The *in vivo* physiological role of ZFP407 in mature adipocytes, however, remains to be elucidated. Here we generated adipocyte-specific ZFP407 knockout (AZKO) mice and discovered a partial lipodystrophic phenotype with reduced fat mass, hypertrophic adipocytes in inguinal and brown adipose tissue, and reduced adipogenic gene expression. The lipodystrophy was further exacerbated in AZKO mice fed a high-fat diet. Glucose and insulin tolerance tests revealed decreased insulin sensitivity in AZKO mice compared to control littermates. Cell-based assays demonstrated that ZFP407 is also required for adipogenesis, which may also contribute to the lipodystrophic phenotype. These results demonstrate an essential *in vivo* role of ZFP407 in brown and white adipose tissue formation and organismal insulin sensitivity.

1. Introduction

Obesity is a global public health problem, given its association with comorbidities such as type 2 diabetes and cardiovascular disease, both of which increase the risk for premature mortality. Obesity is associated with imbalances between energy expenditure and energy storage, resulting in increased lipid deposition. Adipocytes are the body's primary site of physiological energy storage and are vital for integrating and communicating metabolic signals such as those that control glucose metabolism. The depletion of adipocytes leads to insulin resistance, glucose intolerance, hyperinsulinemia and hepatosteatosis (Sakaguchi et al., 2017). Thus, adipocytes are a key target for preventing and treating obesity and type 2 diabetes.

Peroxisome proliferator-activated receptor γ (PPARγ) is a member of the nuclear hormone receptor family of ligand-inducible transcription factors (Tontonoz and Spiegelman, 2008) and is critical to the pathophysiological and pharmacological treatment of insulin resistance

(Kersten et al., 2000). PPARγ expression is highest in adipocytes where it is necessary for differentiation, and is therefore considered a master regulator of adipogenesis as well as a key regulator of gene expression in mature adipocytes (Hu et al., 1995; Tontonoz et al., 1994). *PPARG* mutations cause lipodystrophy in humans (Agarwal and Garg, 2002; Barroso et al., 1999; Hegele et al., 2002; Savage et al., 2003; Visser et al., 2011), which is associated with severe insulin resistance (Melvin et al., 2018). Global knockout of PPARγ in mice is embryonic lethal as it is required for placental and cardiac development (Barak et al., 1999). However, PPARγ knockout mice whose viability was rescued by expression in trophoblast cells, as well as adipocyte-specific PPARγ knockout mice have a lipodystrophic phenotype, including insulin resistance and elevated triglycerides (Duan et al., 2007; He et al., 2003; Wang et al., 2013). Therefore, PPARγ deficiency in both humans and model organisms impairs the transcriptional control of adipogenesis and mature adipocyte viability resulting in lipodystrophy and the resulting metabolic disorders.

Zinc finger protein 407 (ZFP407) was first identified as a positive regulator of insulin-stimulated glucose uptake in 3T3-L1 adipocytes (Buchner et al., 2015). *Zfp407* encodes a 246-kDa protein with 24 zinc finger domains. ZFP407 deficiency in adipocytes reduced insulin-stimulated glucose uptake and decreased expression of PPARγ target genes, including the glucose transporter GLUT4 (Buchner et al., 2015). Studies of a transgenic mouse strain that overexpressed ZFP407 primarily in muscle and heart tissue found that PPARγ target genes, including *Glut4*, were significantly upregulated in these tissues. Furthermore, ZFP407 overexpression improved glucose homeostasis and prevented many of the metabolic disturbances resulting from an obesogenic diet (Charrier et al., 2016). However, the *in vivo* physiological role of ZFP407 in adipocytes remains poorly understood.

In the current study, adipocyte-specific ZFP407 knockout (AZKO) mice were generated using the Adipoq-cre transgene (Lee et al., 2013) to specifically delete ZFP407 in both white and brown adipocytes. We demonstrate that mice lacking ZFP407 in adipocytes exhibit a partial lipodystrophic phenotype and decreased insulin sensitivity, consistent with a repressed PPARγ phenotype. Thus, these studies demonstrate that ZFP407 is required for adipose tissue formation and optimal organismal insulin sensitivity.

2. Materials and methods

2.1. Mice

Embryonic stem (ES) cell clone EUCF0081C12, derived from ES cell strain E14, was obtained from the European Conditional Mouse Mutagenesis Program (Friedel et al., 2007). This clone carried a gene-trap construct integrated in intron 4 of *Zfp407* designed to first be a knockout gene, but contain conditional potential with additional crosses (Fig. 1A) (Schnutgen et al., 2005). This cell line was determined to be euploid and chimeric mice for the conditional allele of *Zfp407* were generated. FVB mice were used as embryo hosts for ES cell injection and C57BL/6J females were used as pseudopregnant recipients. Chimeric founder mice were identified by their coat color (black), were verified by genotyping of their offspring, and were subsequently maintained by serial backcrossing to strain C57BL/6J. Mice utilized in this study were from backcross generations N7 – N14.

To generate a conditional allele of *Zfp407*, mice that were heterozygous for the knockout-first allele of *Zfp407*^{+/−} were mated with

ROSA26::FLPe (Strain B6.129S4-Gt(ROSA)26Sor[tm1(FLP1)Dym]/RainJ; Stock #009086, The Jackson Laboratory, Bar Harbor, ME, USA). Offspring from this cross that inherited the *Flpe* transgene and the *Zfp407* mutant allele now carried the equivalent of a *Zfp407* floxed allele, as the FLPe inverted and thereby inactivated the gene trap allele. The flipped and therefore inactive gene trap allele remained flanked by *LoxP* sites in opposite orientations enabling conditional inversion by Cre recombinase (Farley et al., 2000). To generate adipose-specific deficiency of ZFP407, mice carrying the *Zfp407* floxed allele (*Zfp407*[flox/+]) were mated with Adipoq-Cre mice (B6; FVB-Tg(Adipoq-cre)1Evdr/J; Stock #010803, The Jackson Laboratory, Bar Harbor, ME, USA) (Eguchi et al., 2011).

Mice were housed in ventilated racks with access to food and water *ad libitum* and maintained at 21 °C on a 12-h light/12-h dark cycle. All mice were cared for as described under the Guide for the Care and Use of Laboratory Animals of the National Institute of Health, eighth edition (2011) and all experiments were approved by IACUC and carried out in an AAALAC approved facility. Mice were fed standard chow diet LabDiet 5010 unless otherwise indicated (PMI Nutrition International, St. Louis, MO, USA). For dietary studies mice were fed either a high fat/high sucrose diet (HFD) with 58% of kcal from fat or a nutritionally balanced control diet (CD) with 10.5% of kcal from fat (HFD: D12331; CD: D12328, Research Diets, New Brunswick, NJ, USA). *Zfp407*^{+/+}, Adipoq-Cre mice as well as *Zfp407*[flox/flox] mice without the Cre transgene, and *Zfp407*^{+/+} littermates were used as controls for all mouse experiments. For metabolic studies, mice were fasted 16 h overnight and blood glucose levels were measured via retro orbital bleeds. Whole blood was collected by cardiac puncture using BDmicrotainer tubes with K₂ EDTA. For tissue collection, mice were anesthetized with isoflurane and euthanized by cervical dislocation at approximately 9 a.m. (ZT3). Tissues were either snap frozen in liquid nitrogen or placed in 4% paraformaldehyde.

2.2. Blastocyst DNA preparation

Male and female *Zfp407*^{+/−} mice were placed together in mating pairs at 5 p.m. At 8 a.m. the following morning, females were checked for plugs and isolated from male mates. The 12 p.m. on this same day was assumed to be the Day 0.5 post-fertilization time point. Three days following, females were sacrificed (Day 3.5) and adipose tissue surrounding the uterus was completely removed. Uterine horns were
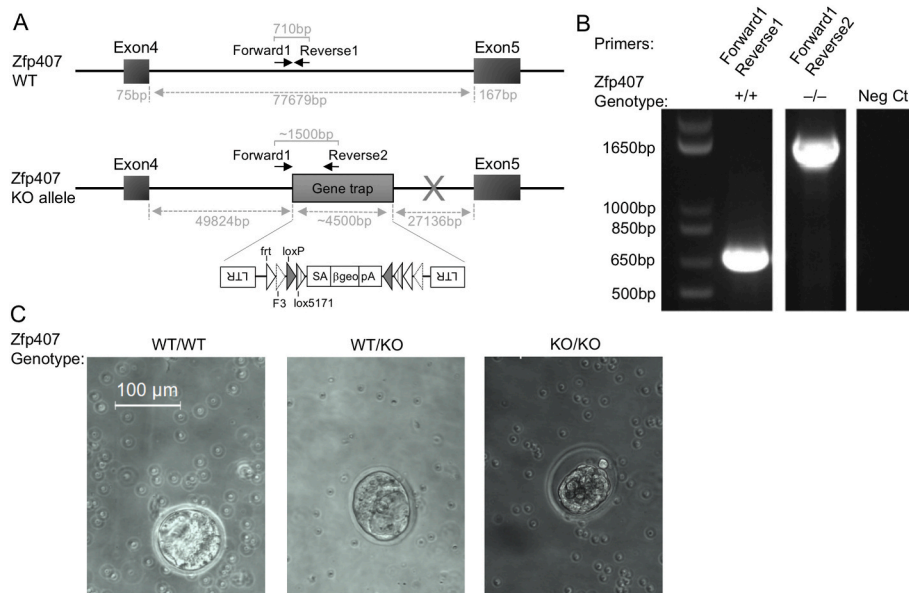
Fig. 1. ZFP407 is required for embryogenesis in mice. (A) Schematic representation of the wild-type *Zfp407* genomic loci and *Zfp407* gene trapped genomic loci. The gene trap cassette is located in intron 4, which contains LTR (long terminal repeat); heterotypic target sequences for the FLPe recombinase: frt (triangles) and F3 (triangles with dotted line); heterotypic target sequences for the Cre recombinases: loxP (solid triangles) and lox5171 (strip filled triangles); splice acceptor (SA); β-galactosidase/neomycin phosphotransferase fusion gene (βgeo); bovine growth hormone polyadenylation sequence (pA). Primers used to distinguish wild-type and knockout alleles are indicated. (B) Genotyping results detecting the presence of the wild-type allele (*Zfp407*^{+/+}, 710 bp fragment) in lane 2 and the knockout allele (*Zfp407*^{−/−}, ~1500 bp) in lane 3. ddH₂O was used as the PCR template as a negative control (Neg Ctl) in lane 4. The 1 Kb Plus DNA ladder is shown in lane 1 (ThermoFisher Scientific, Waltham, MA, USA). (C) Representative blastocyst images from *Zfp407* wild-type (+/+), heterozygous (+/−) and knockout (−/−) embryos illustrating abnormal blastocyst formation cause by ZFP407 deficiency.

isolated and flushed using MilliporeSigma EmbryoMax FHM HEPES Buffered Medium 1X (ThermoFisher Scientific, Waltham, MA, USA) under a dissecting microscope. Blastocysts were photographed and separated into 1.7 mL tubes. DNA was isolated from blastocysts using a Qiagen DNeasy Blood and Tissue Kit (Qiagen, Germantown, MD, USA) following a brief incubation at 53 °C in Proteinase K.

2.3. Genotyping

Blastocyst genotyping for the *Zfp407* wild-type (WT) or knockout (KO) alleles was performed using nested PCR. The initial round of PCR was performed on isolated blastocyst DNA using Q5 Hot Start High Fidelity Polymerase (New England Biolabs, Ipswich, MA, USA) according to the manufacturer's protocol with long-range primers designed to amplify a ~6.6 kb region of DNA that included the entire gene trap inserted into intron 4 of the *Zfp407* gene (as described above). The *Zfp407* long-range primer sequences are as follows: Forward 5′-CAACC AACCA GCCAG TGAGA T-3′ and Reverse 5′-CAAAC AATTG GGGAA AGTGA-3′. Following amplification, PCR products were purified using the PureLink PCR Purification Kit (ThermoFisher Scientific, Waltham, MA, USA) according to manufacturer's protocol. For the nested round of PCR, two sets of primers were used. The first set amplifies a ~1500 bp fragment in mice carrying the gene trapped allele of *Zfp407*. The sequences for these primers are as follows: Forward 1: 5′-CTGAG CTGAT GTGCT CCTGT-3′; Reverse 1: 5′- GAATA GGAAC TTCGG AATAG GAA-3′. The second set of primers amplifies a 710 bp fragment in mice carrying a wild type allele of *Zfp407*. These primer sequences are as follows: Forward 2: 5′-TGCAG TAAGG CTCTG CTGTC-3′; Reverse 2: 5′-GGCCT GCAAA ATGAG TCCTA-3′. Using both sets of primers to genotype each blastocyst, all three possible blastocyst genotypes ($+/+$, $+/-$ or $-/-$) were determined. The *Zfp407* gene trapped allele was genotyped in mice using a single 3-primer PCR reaction with the primers Forward 1, Reverse 1, and Reverse 2 to amplify the 710 and ~1500 bp fragments as previously described for the blastocyst genotyping assay.

AZKO and littermate control mice were genotyped using 3 PCR reactions to detect: 1) a ~350 bp fragment indicative of the *Zfp407* WT allele, 2) an ~800 bp fragment indicative of the *Zfp407* floxed allele, and 3) a ~300 bp fragment indicative of the Adipoq-cre transgene. PCR primers used were: (#1) *Zfp407* WT primers: Forward: 5′-TGCAG TAAGG CTCTG CTGTC-3′, Reverse: 5′-GGCCT GCAAA ATGAG TCCTA-3′. (#2) *Zfp407* gene trap primers: Forward: 5′-TGCAG TAAGG CTCTG CTGTC-3′, Reverse: 5′-ATTGC ATCGC ATTGT CTGAG-3′. (#3) *Cre* primers: Forward: 5′-GTTCG CAAGA ACCTG ATGGA C-3′ and Reverse: 5′-CTAGA GCCTG TTTGC ACGTT-3′.

2.4. Histology

Fixed adipose tissue was embedded in paraffin, cut into 4 μm sections and stained with hematoxylin and eosin. Images were acquired by brightfield microscopy (DM6000, Leica Biosystems, Buffalo Grove, IL, USA). Adipocyte number and area were measured using ImageJ software (NIH; n = 3 mice per group, and 3 images per mouse were analyzed).

2.5. Western blotting

Western blotting was performed and quantitated as described (Buchner et al., 2015). Anti-PPARγ antibody was obtained from Bethyl Laboratories (#A304-461A, Montgomery, TX, USA), and anti-GAPDH was from Proteintech Group (#60004-1, Rosemont, IL, USA). A custom anti-ZFP407 antibody was generated in rabbit against the C-terminal 149 amino acids of the mouse ZFP407 protein (Proteintech Group, Rosemont, IL, USA). Goat anti-rabbit (#31460) and goat anti-mouse (#31430) secondary antibodies were obtained from ThermoFisher Scientific (Waltham, MA, USA).

2.6. Cell culture

3T3-L1 cells were passaged and differentiated as previously described (Chiang et al., 2006). For shRNA knockdown experiments, lentiviral particles expressing either a control shRNA (pLKO.1, Sigma-Aldrich, St. Louis, MO, USA) or an shRNA targeting *Zfp407* (TRCN238954, Sigma-Aldrich, St. Louis, MO, USA) were prepared and propagated in HEK293T cells as described previously (Guan et al., 2017) using the second generation of psPAX2 and pMD2.G packaging vectors. After two rounds of lentiviral infection, cells were then cultured and differentiated as previously described (Roy et al., 2017).

2.7. Mouse stromal vascular fraction (SVF) isolation and culture conditions

Mouse subcutaneous and gonadal fat pads were removed from 8-week-old C57BL/6J mice. Tissues were minced and digested in 10 mL digestion buffer (1% BSA, 2 mM $CaCl_2$ in KRB buffer, 300 U/mL collagenase), filtered by 40 μm cell strainers, and centrifuged to collect SVF cells in the pellet. The SVF was seeded on collagen-coated plates and cultured in DMEM/F12 medium supplemented with 10% FBS, 100 IU penicillin and 100 μg/mL streptomycin. Once cells reach 30–40% confluency, lentivirus particles expressing shRNA targeting *Zfp407* or control shRNA were added to the medium and incubated for 24 h. After two rounds of infection, cells were cultured in growth medium until confluence. Cells were then induced to differentiate for 4 days with DMEM/F12 medium containing 10% FBS, 100 IU penicillin, 100 μg/mL streptomycin, 5 μM dexamethasone, 0.5 μg/mL insulin, 0.5 mM IBMX (Sigma-Aldrich, St. Louis, MO, USA) and 1 μM rosiglitazone (Cayman Chemical, Ann Arbor, MI, USA). The induction medium was replaced with DMEM/F12 medium containing 10% FBS, 100 IU penicillin, 100 μg/mL streptomycin and 0.5 μg/mL insulin for another 4 days.

2.8. ELISA

An Ultra Sensitive Mouse Insulin ELISA Kit (Crystal Chem, Downers Grove, IL, USA) was used according to manufacturer's protocol for the wide range assay to measure plasma insulin levels.

2.9. Glucose and insulin tolerance test

Following 86 days on the HFD or CD, mice were fasted overnight for 16 h, blood samples were collected by tail vein nick, and glucose levels were measured with a handheld glucometer at baseline (time 0) and following intraperitoneal injection of dextrose (2 g/kg body weight) or insulin (1U/kg body weight) dissolved in water or PBS, respectively. The homeostasis model for insulin resistance (HOMA-IR) was calculated from the fasting blood glucose (mmol/L) × fasting plasma insulin (μU/mL) divided by 22.5.

2.10. Statistics

Data are shown as the mean ± standard error unless otherwise indicated. Western blot data was analyzed by two-tailed Student's *t*-test. Fat pad weights, mouse weights, mouse lengths, mouse fasting glucose, mouse fasting insulin, and area under the curve for glucose and insulin tolerance tests were analyzed by a three-way ANOVA for effects of genotype, diet, and sex and further analyzed stratified by sex by Student's *t*-test followed by Bonferroni's correction for multiple comparison (Table 1). For all physiological parameters listed in Table 1, a sample size of $n \geq 75$ was considered large enough to assume normal distribution by histogram visualization. When the sample sizes were $n < 75$, a Shapiro-Wilk test for normal distribution was performed on the residuals of the ANOVA analysis. If a trait failed normality ($P < 0.05$), then values were reshaped by taking the natural log. The reshaped values all passed the Shapiro-Wilk test for normal distribution, and so ANOVA was

Table 1
Metabolic trait data for CD- or HFD-fed control and AZKO mice.

Trait	CD control mean	SE	n	AZKO mean	SE	n	HFD control mean	SE	n	AZKO mean	SE	n	3 way ANOVA (p value) Genotype	Diet	Sex	Interactionss
Female																
body weight, g	21.88	0.96	10	21.23	0.64	8	25.77	0.90	15	25.50	1.60	7	2.99E-03	7.87E-08	2.00E-16	NS
inguinal fat mass, g	0.18	0.01	10	0.05	0.01	8	0.46	0.07	14	0.12	0.02	7	3.91E-07	1.75E-07	NS	NS
epididymal fat mass, g	0.16	0.01	10	0.11	0.02	8	0.35	0.06	15	0.27	<0.01	7	3.13E-07	5.81E-06	1.79E-05	Genotype/Sex, p = 2.81E-04
BAT mass, g	0.05	<0.01	10	0.02	<0.01	8	0.06	<0.01	15	0.02	<0.01	7	2.00E-16	NS	2.39E-07	NS
fasting insulin, ng/mL	0.39	0.14	9	0.45	0.12	4	0.46	0.17	9	0.54	0.07	8	NS	NS	NS	NS
fasting glucose, mg/dL	79.89	4.26	9	129.75	10.25	4	102.22	5.26	9	128.13	7.60	8	3.95E-04	3.95E-04	NS	NS
HOMA-IR	1.11	0.41	9	1.91	0.44	4	1.56	0.54	9	2.49	0.41	8	NS	NS	NS	NS
GTT AUC	1152	51	12	1347	30	8	1265	47	13	1271	61	6	NS	7.07E-05	NS	NS
ITT AUC	2.14	0.14	10	2.79	0.16	7	2.08	0.08	13	2.78	0.15	7	1.23E-08	NS	NS	NS
Male																
body weight, g	29.60	0.68	17	27.02	0.50	7	33.25	0.79	20	32.76	1.29	7	2.99E-03	7.87E-08	2.00E-16	NS
inguinal fat mass, g	0.29	0.02	17	0.08	0.02	7	0.54	0.07	20	0.38	0.06	7	3.91E-07	1.75E-07	NS	NS
epididymal fat mass, g	0.42	0.04	17	0.06	0.01	7	0.93	0.12	20	0.22	0.03	7	3.13E-07	5.81E-06	1.79E-05	Genotype/Sex, p = 2.81E-04
BAT mass, g	0.07	0.01	17	0.03	<0.01	7	0.08	0.01	20	0.03	0.01	7	2.00E-16	NS	2.39E-07	NS
fasting insulin, ng/mL	0.21	0.06	11	0.21	0.04	7	0.30	0.05	13	0.47	0.24	8	NS	NS	NS	NS
fasting glucose, mg/dL	87.82	6.49	11	103.57	9.80	7	118.31	10.66	13	125.50	6.19	8	3.95E-04	3.95E-04	NS	NS
HOMA-IR	0.68	0.23	11	0.74	0.11	7	1.28	0.24	13	2.28	1.25	8	NS	NS	NS	NS
GTT AUC	1249	53	19	1132	98	8	1454	49	21	1511	54	9	NS	7.07E-05	NS	NS
ITT AUC	2.28	0.15	13	2.80	0.08	5	2.12	0.11	19	2.87	0.13	6	1.23E-08	NS	NS	NS

CD, control diet; HFD, high-fat diet; BAT, brown adipose tissue; GTT AUC, glucose tolerance test area under the curve; ITT AUC, Insulin tolerance test area under the curve; NS, Not significant.

performed on these values. *P* values < 0.05 were considered statistically significant for all statistical tests.

3. Results

3.1. ZFP407 is necessary for embryogenesis in mice

A ZFP407 KO mouse strain with conditional potential was generated from ES cells carrying a gene-trap construct in intron 4 of the *Zfp407* locus (Fig. 1A–B). The gene-trap introduced a new splice acceptor site to which the endogenous *Zfp407* transcript is spliced following exon 4. The gene-trap construct contains a premature termination codon, thus the gene-trapped allele of *Zfp407* is predicted to encode a truncated protein that is missing the C-terminal 630 amino acids from a 2246 amino acid protein. The truncated portion of the protein is predicted to encode six of the zinc finger domains within ZFP407, and was thus expected to encode a null allele (Schnutgen et al., 2005).

Heterozygous *Zfp407* mutant mice (+/−) were viable with no obvious morphological defects (Chi-square: p > 0.84) (Table 2). However, when *Zfp407$^{+/−}$* mice were intercrossed, no *Zfp407* KO mice (−/−) were observed at weaning (Table 2). To further determine the developmental stage at which ZFP407 was required for viability we performed timed matings and embryos were genotyped at various time points between embryonic stages E6.5 and E18.5. The absence of *Zfp407$^{−/−}$* embryos was detected as early as E6.5 (Chi-square: P <

Table 2
Survival of Zfp407 deficient mice at various ages.

Backcross: Zfp407 +/− x +/+				
Zfp407 genotype	+/+	+/−	total	p value
3 weeks	219	215	434	0.848
Expected ratio	1	1		

Intercross: Zfp407 +/- x +/-				
Zfp407 genotype	+/+	+/−	−/−	p value
e18.5–3 weeks	29	32	0	<0.00001
e6.5-e18.5	17	28	0	0.00042
Blastocysts	32	15	2	<0.00001
Expected ratio	1	2	1	

0.0001, Table 2). To test for viability at even earlier embryonic stages, blastocysts from the *Zfp407$^{+/−}$* intercross were collected and genotyped. Although *Zfp407$^{−/−}$* blastocysts were detected, they were significantly underrepresented among offspring of a *Zfp407$^{+/−}$* intercross (Table 2), with the few observed blastocysts presenting with significant morphological abnormalities, including a shrunken and fragmented appearance (Fig. 1C). It is potentially of note that there was also a deficiency of

heterozygous mice among offspring of the *Zfp407*^{+/−} intercross, however this was not observed in the *Zfp407*^{+/−} backcross (Table 2). Mendelian frequencies of wild type and heterozygous mice were observed in offspring of the backcross regardless of whether the male or female parent was heterozygous, suggesting that *Zfp407*^{+/−} parents do not impair viability of heterozygous offspring. Thus, it remains unclear why there was a deficiency of *Zfp407*^{+/−} mice from the intercross, but may just be due to random fluctuations given the smaller sample size of intercross offspring relative to the backcross. Nonetheless, these crosses demonstrate that ZFP407 is required for embryonic development, as it is essential for proper blastocyst development.

3.2. Generation of AZKO mice

Given the early embryonic lethality caused by whole body ZFP407 deficiency, as well as the role of ZFP407 in PPARγ signaling and insulin sensitivity (Buchner et al., 2015; Charrier et al., 2016), we sought to specifically test the *in vivo* physiological role of ZFP407 in adipocytes by generating an adipocyte-specific ZFP407 KO mouse (AZKO; Fig. 2A). To do this, *Zfp407*^{+/−} mice were crossed to a mouse expressing FLPe recombinase (Eguchi et al., 2011), resulting in an inversion and therefore inactivation of the gene-trap construct. In this orientation the gene-trap is flanked by *LoxP* sites in opposite orientation, which in the presence of Cre recombinase will undergo inversion of the gene-trap cassette and deletion of one of the *LoxP* sites, returning the gene-trap to its original orientation and stably inactivating *Zfp407*. Thus, following FLPe-mediated inversion, this allele is functionally equivalent to a "floxed" allele and will be referred to as such.

To generate AZKO mice, mice carrying the floxed allele of *Zfp407* were bred over the course of two generations to mice expressing Cre recombinase under the control of the *Adiponectin* promoter (Eguchi et al., 2011) which drives expression specifically in white and brown adipocytes (Mullican et al., 2013). The *Zfp407*[flox/flox], Adiponectin Cre + offspring, and all other offspring genotypes, were detected at the expected Mendelian ratios (Chi-squared: P > 0.79, Table 3). Mice that were homozygous for the floxed *Zfp407* allele, which did not carry the Cre transgene (*Zfp407*[flox/flox]; Adiponectin Cre–), as well as *Zfp407*^{+/+}, Adipoq-Cre mice, and *Zfp407*^{+/+} littermates were used as controls (Fig. 2A–B, Figure S1). Since βgeo is expressed from the gene-trap cassette when in the knockout orientation, we tested for β-gal mRNA expression to assess the specificity of *Zfp407* KO among tissues. β-gal

Table 3
Survival of offspring from the Zfp407-fl/+, Cre +, x Zfp407-fl/+ cross to generate AZKO mice.

Zfp407 genotype	+/+	+/+	fl/ +	fl/ +	fl/ fl	**fl/ fl**	total	P value
Cre genotype	−	+	−	+	−	**+**		
observed	92	74	172	171	90	**83**	682	0.7977
Expected ratio	1	1	2	2	1	**1**		

For Zfp407 genotypes, fl indicates the floxed allele and + indicates the wild type allele.

For Cre genotype, + indicates presense of the transgene and - indicates absence of the transgene.

AZKO mice are indicated in bold.

levels were dramatically increased in subcutaneous, gonadal and brown adipose tissues of AZKO mice relative to non-adipose tissues (Figure S2), demonstrating the adipose-specific nature of the Zfp407 knockout. ZFP407 protein levels were decreased ~50% in the subcutaneous and brown fat pads of AZKO mice. Since adipose tissue contains many non-adipocyte cell types, it is likely that much of the residual ZFP407 expression detected in adipose tissue of AZKO mice is from cells other than adipocytes. Although ZFP407 was significantly reduced in subcutaneous and brown fat pads, there was no difference in ZFP407 protein levels in gonadal fat pads (Fig. 2C). Although the Adiponectin-cre transgene has been shown to delete floxed alleles with equal efficiency in both gonadal and subcutaneous adipocytes (Lee et al., 2013), the genomic context of each floxed allele is unique. The presumed higher efficiency of Cre-mediated deletion of *Zfp407* in subcutaneous adipocytes is associated with significantly higher levels of ZFP407 in subcutaneous relative to gonadal adipose tissue (~15-fold higher) (Buchner et al., 2015), and may therefore reflect a more open chromatin structure on which the Cre recombinase can act.

3.3. Adipocyte-specific ZFP407 knockdown results in lipodystrophy

Fat pads from AZKO and control mice fed a chow diet were weighed and sections of these tissues were stained by hematoxylin and eosin. Fat pads weighed significantly less in AZKO mice, with a ~75% reduction in both inguinal white adipose depots and brown adipose tissue weight (Fig. 3A). There was no statistically significant decrease in epididymal adipose tissue weight, although it also trended lower in AZKO mice
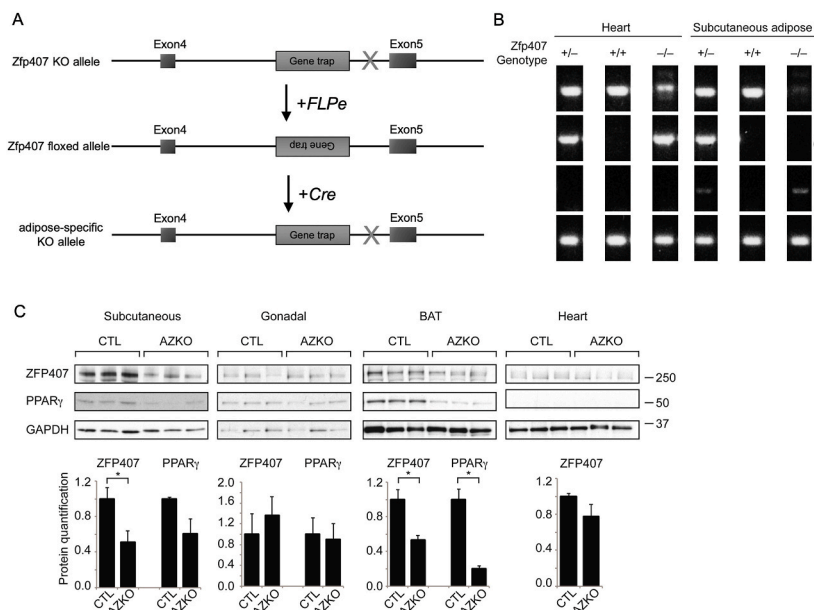
Fig. 2. Generation of AZKO mice. (A) Schematic representation illustrating each stage of the conditional *Zfp407* allele associated with insertion of a gene trap cassette within intron 4 of the *Zfp407* locus. Initially, the gene trap functions as a knockout allele as the gene trap is in the forward orientation in all cells (KO allele). Upon inversion of the gene trap, *Zfp407* reverts to its normal expression in all cells (floxed allele). Finally, upon Cre-mediated inversion of the gene trap allele, *Zfp407* reverts to a knockout allele specifically in the Cre-expressing cells, which in this case are adipocytes (adipocyte-specific KO allele). (B) Genotyping results from DNA isolated from heart and subcutaneous adipose tissue in wild-type, floxed, gene-trapped, and AdipoQ-Cre mice. AZKO mice are indicated by the absence of the WT- and floxed-specific PCR products and the presence of the KO-specific PCR product. (C) Immunoblot of ZFP407 and PPARγ in various fat depots and heart tissue from control and AZKO mice. GAPDH serves as the loading control. Protein quantifications were normalized to GAPDH levels, $n = 3$ mice/group, *$P < 0.05$.
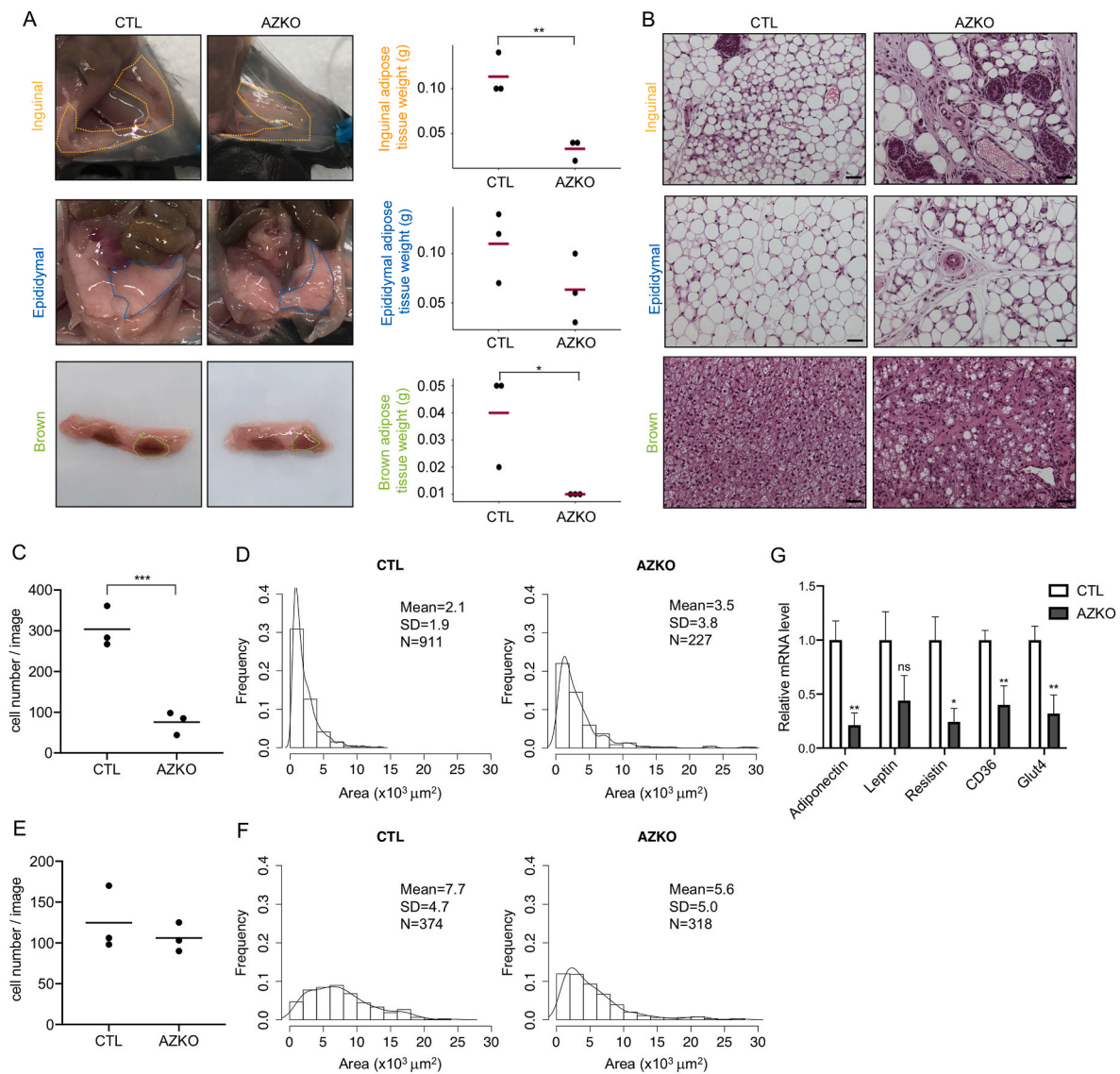
Fig. 3. ZFP407 ablation in adipose tissue leads to lipodystrophy. (A) Gross morphology and weight changes of inguinal (*orange dotted line*), epididymal (*blue dotted line*), and brown (*green dotted line*) adipose tissue from control and AZKO female mice. (B) H&E staining of these adipose tissues; scale bar, 50 μm. (C) Quantification of adipocyte number per image from inguinal adipose tissues. (D) Histogram showing distribution of adipocyte area of inguinal adipose tissues from control and AZKO mice. (E) Quantification of adipocyte number per image from epididymal adipose tissues. (F) Histogram showing distribution of adipocyte area of epididymal adipose tissues from control and AZKO mice. Each distribution is obtained from three female mice/group in (D) and (F), with 3 images per mouse analyzed. (G) mRNA levels of adipokine and adipogenic genes in inguinal fat depots. $n = 7$–8 mice/group $*P < 0.05$, $**P < 0.01$, $***P < 0.001$, ns, not significant.

(CTL: 0.11g vs. AZKO: 0.06g, p = 0.18). Major histological differences were observed in both inguinal white adipose tissue and brown adipose tissue between AZKO and control mice. In addition to the smaller adipose tissue depots, the inguinal fat depots from AZKO mice contained a smaller percentage of adipocytes among the remaining cells, with a concomitant increase in vasculature and connective tissue cells (Fig. 3B). The remaining adipocytes tended to be larger in size, containing brightly eosinophilic cytoplasm or very large unilocular vacuoles, which together with the smaller adipose depots, is consistent with a dramatic loss of adipocytes due to cell death, or trans- or de-differentiation (Fig. 3B–D). There was no significant difference in epididymal adipocyte size (Fig. 3E and F), while the brown fat depots in AZKO mice displayed a higher frequency of white adipocyte-like cells, also consistent with loss of most of the brown adipocytes (Fig. 3B).

We next examined the effects of ZFP407 ablation on adipocyte marker gene and adipokine expression levels. Consistent with the reduction in fat mass, *Leptin*, *Adiponectin* and *Resistin* mRNA levels in inguinal fat depots were markedly decreased in AZKO mice (Fig. 3E).

The mRNA expression levels of adipocyte markers *Cd36* and *Glut4* (Fig. 3E), as well as protein levels of PPARγ (Fig. 2C), were also dramatically lower in inguinal fat depots of AZKO mice. The loss of these adipocyte markers is likely secondary to the reduction in adipocytes, as although ZFP407 has previously been shown to alter PPARγ downstream signaling in adipocytes, including GLUT4, it did so without altering levels of PPARγ itself (Buchner et al., 2015; Charrier et al., 2016). Therefore, the reduction in expression of these adipocyte markers suggested an impairment of adipocyte differentiation or an impairment of adipocyte viability.

To explore the potential role of ZFP407 in adipocyte differentiation, 3T3-L1 preadipocytes were transfected with lentivirus containing an shRNA targeting *Zfp407* or a control sequence (Fig. 4A), followed by cellular differentiation as previously described (Chiang et al., 2006). The ability of cells to differentiate, as indicated by lipid droplet formation, was evaluated by Oil Red O staining at the end of the differentiation protocol. ZFP407 knockdown significantly reduced lipid droplet formation, suggestive of attenuated adipocyte differentiation (Fig. 4B),
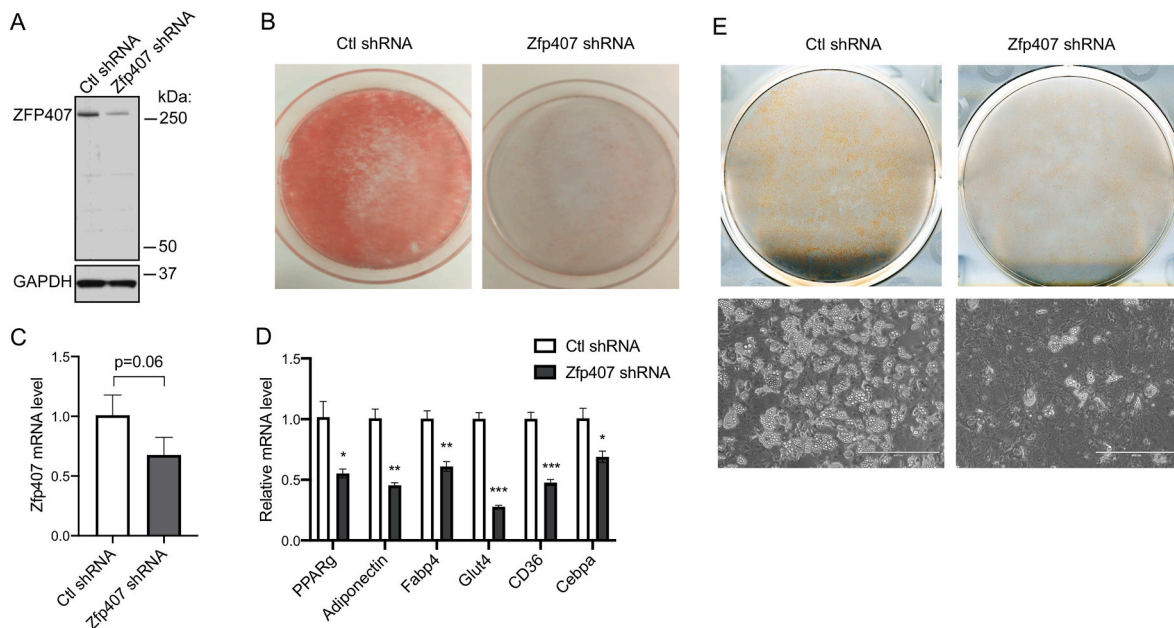
Fig. 4. ZFP407 is a positive regulator of adipocyte differentiation (A) 3T3-L1 cells were infected by lentiviral shRNA targeting *Zfp407* or a control shRNA followed by differentiation for 10 days. Western blot to examine the protein levels of ZFP407. (B) Oil-Red O staining to assess lipid accumulation in 3T3-L1 cells. $n = 4$/group. (C) Mouse SVF cells isolated from subcutaneous white adipose tissue depots (sWAT) were infected by lentiviral shRNA targeting *Zfp407* or a control shRNA followed by differentiation for 8 days. Real-time PCR was used to measure the knockdown efficiency. (D) mRNA levels of adipogenic maker gene expression in SVF cells from sWAT. $*P < 0.05$, $**P < 0.01$, $***P < 0.001$. (E) Lipid accumulation in SVF cells from sWAT shown with photograph of oil-red O staining and bright-field images; scale bar, 400 μM $n = 3$/group.

consistent with the reduced gene expression of adipogenic genes observed in AZKO mice *in vivo* (Fig. 3G). To further investigate the cell autonomous role of ZFP407 in adipogenesis, ZFP407 was depleted in SVF isolated from subcutaneous white adipose tissue depots and gonadal white adipose tissue depots of 8-week-old C57BL/6J mice. The pre-adipocytes were transfected with lentivirus containing an shRNA targeting *Zfp407* or a control shRNA, and induced to differentiate (Fig. 4C and Figure S3A). Knocking down *Zfp407* in SVF differentiated from both subcutaneous and gonadal depots significantly decreased adipocyte marker gene expression, including *Adiponectin*, *Glut4*, *Fabp4*, among others (Fig. 4D and Figure S3B). In addition, lipid accumulation was also significant reduced (Fig. 4E). Collectively, these data show that ZFP407 is required for adipogenesis in both subcutaneous and gonadal white adipose tissue depots.

3.4. Lipodystrophy in HFD-fed AZKO mice

To determine the role of adipocyte-derived ZFP407 in organismal physiology under obesogenic conditions, AZKO and control mice were fed a high fat diet (HFD: 58% kcal from fat) or a nutritionally balanced control diet (CD: 10.5% kcal from fat) for 100 days beginning at 5 weeks of age. When fed a HFD, AZKO and control mice both increased their body weight by 15%–20%, with no significant differences between the two groups in total body weight (Fig. 5A–B). With respect to adipose tissue specifically, the HFD significantly increased inguinal and epididymal fat pad weights in control mice, however, these gains were muted in AZKO mice (Fig. 5C–D). Brown adipose tissue depots were also smaller and weighted less in AZKO mice relative to control mice fed either the HFD or CD (Fig. 5E–F). Impaired tissue morphology was detected in the inguinal, epididymal and brown adipose tissue depots of AZKO mice, and was further exacerbated by the HFD (Fig. 3B, Figure S4). These data suggest that adipocyte cell death may mediate the loss of white and brown adipose tissue, leading to partial lipodystrophy in AZKO mice, with the differences between AZKO and control mice even further magnified in mice fed the HFD.

3.5. AZKO mice have reduced insulin sensitivity

Lipodystrophy often leads to insulin resistance and glucose intolerance due to the excess storage of lipids in non-adipose tissues (Cortes and Fernandez-Galilea, 2015; Fiorenza et al., 2011; Mann and Savage, 2019; Melvin et al., 2018). Although the adipose tissue alterations in AZKO mice were largely restricted to the inguinal rather than epididymal fat depots, we nonetheless sought to assess whether this partial lipodystrophy in AZKO mice was associated with impaired organismal insulin sensitivity in both CD- and HFD-fed mice. No significant changes in fasting insulin or HOMA-IR scores were observed between the CD-fed or HFD-fed AZKO and control mice (Fig. 6A–B). However, fasting plasma glucose levels were increased in AZKO female mice relative to controls when fed with CD (Fig. 6A, Table 1). To further investigate insulin sensitivity using a more sensitive assay, glucose and insulin tolerance tests were performed. Although no defects in insulin sensitivity were detected with the glucose tolerance tests, AZKO mice exhibited decreased hypoglycemic response to insulin compared to control littermates in both female and male mice (Fig. 6C–F). Collectively, these results suggest a mild impairment in insulin sensitivity in AZKO mice, consistent with the partial lipodystrophy.

4. Discussion

These studies have collectively identified essential roles for ZFP407 in embryonic development, adipose tissue formation, and organismal insulin sensitivity. ZFP407 deficiency was lethal at or before the blastocyst stage suggesting a critical role in early organismal development. Little is known about the cellular functions of ZFP407 that may cause such early lethality, although it does regulate the PPARγ signaling pathway (Buchner et al., 2015; Charrier et al., 2016) as well as contribute to cell proliferation and colorectal cancer metastasis downstream of WDR5 (Tan et al., 2017). The early embryonic lethality is not consistent solely with its role in PPARγ signaling, given that the PPARγ knockout mouse is not lethal until E10, due to impaired trophoblast cell function (Barak et al., 1999). However, ZFP407 regulates the activity of
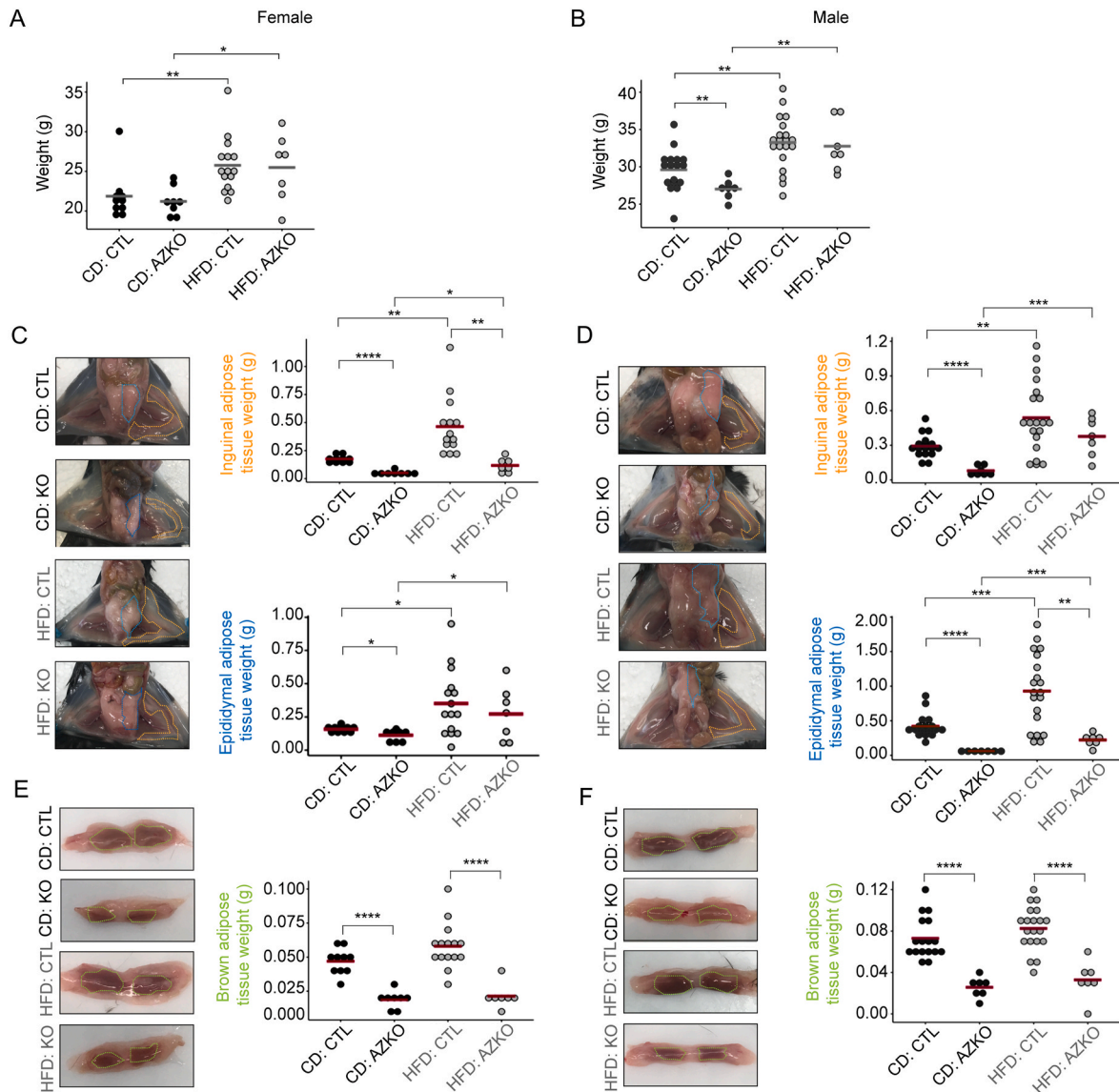
Fig. 5. Effects of HFD on adiposity in AZKO mice. (A) Body weight of control and AZKO female and (B) male mice fed with control diet (CD) or high-fat diet (HFD). (C) Gross morphology and weight changes of inguinal (*orange dotted line*) and epididymal (blue dotted line) from control and AZKO female and (D) male mice fed with CD or HFD. (E) Gross morphology and weight changes of brown (*green dotted line*) adipose tissue from control and AZKO female and (F) male mice fed with CD or HFD. *$P < 0.05$, **$P < 0.01$, ****$P < 0.0001$.

the other PPAR family members PPARα and PPARδ as well (Charrier et al., 2016). Thus, it may be that the early embryonic lethality results from a pan-PPAR deficiency, rather than just the specific loss of PPARγ signaling. It is also possible that the early lethality of ZFP407 deficient embryos is due to its functions downstream of WDR5 or other as yet undiscovered functions. WDR5 is a core component of histone methyltransferase complexes and plays a fundamental role in both transcription and protein synthesis, which as essential cellular processes may be expected to result in an early lethal phenotype (Bryan et al., 2020; Guarnaccia and Tansey, 2018). However, phenotype associated with the loss of function of WDR5 is not yet known.

The early embryonic lethality associated with ZFP407 deficiency is also suggestive that the truncated gene trapped allele encodes a null allele. This suggests that the 6 C-terminal zinc finger domains that are truncated by the gene trap are essential to the function of the protein. ZFP407 is a large protein that contains 24 different C2H2 zinc finger domains, however there is little known about the function of each individual zinc finger domain. The protein structure of ZFP407 is reminiscent of ZFP423, which is another large protein whose domain

structure consists largely of 30 zinc finger domains. ZFP423 is a DNA-binding factor that associates with Smads in response to BMP2, activating *Xvent-2*, and also a transcriptional partner of Olf-1/EBF in olfactory epithelium and lymphocyte development. The 30 zinc fingers are distributed in six clusters, using distinct DNA- and protein-binding characteristics to regulate the BMP-Smad and Olf signaling pathways, thus illustrating the role of a multi-zinc finger protein in integrating distinct signaling transduction pathways during development (Brayer et al., 2008; Hata et al., 2000; Tsai and Reed, 1997, 1998). ZFP407 might also have the potential to facilitate DNA or protein interactions in early embryonic development, however, outside of the necessity of the C-terminal 6 zinc finger domains for viability, it is not yet known what the respective functions are of each of the zinc finger domains or domain clusters in ZFP407. Interestingly, ZFP423 also regulates adipogenesis via PPARγ (Gupta et al., 2010). However, ZFP423 acts as a positive regulator of PPARγ expression (Gupta et al., 2010), whereas ZFP407 acts as a positive regulator of PPARγ activity in the absence of a direct effect on PPARγ expression (Buchner et al., 2015). Despite the mechanistic differences, adipocyte-specific loss of ZFP407 and ZFP423 both result in
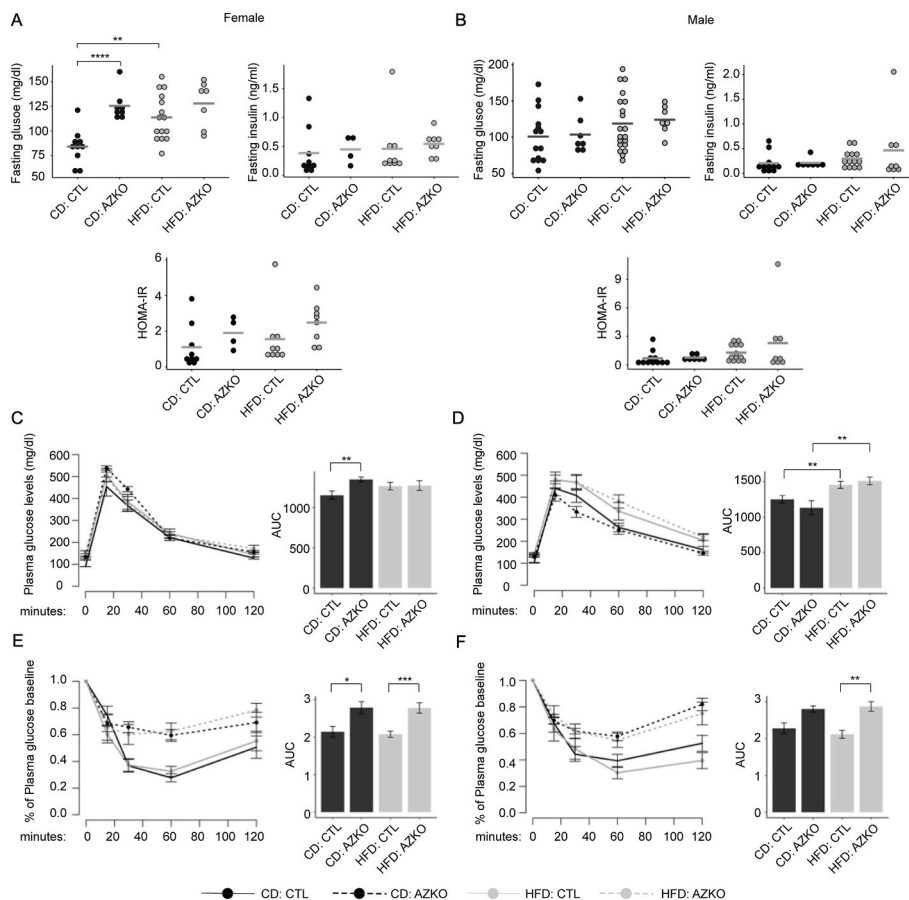
Fig. 6. Insulin resistance in AZKO mice. (A) Plasma glucose and insulin levels in female and (B) male mice fasted for 16 h. Homeostatic model assessment of insulin resistance (HOMA-IR) is also shown. (C) Plasma glucose concentrations for glucose tolerance tests (GTT) in female and (D) male mice fasted for 16 h. (E) Plasma glucose concentrations for insulin tolerance tests (ITT) in female and (F) male mice fasted for 16h. Area under curve (AUC) is also quantified. $n = 7$–20 mice/group. *$P < 0.05$, **$P < 0.01$, ***$P < 0.001$, ****$P < 0.0001$.

impaired adipocyte differentiation and insulin resistance (Shao et al., 2017). Defects in another zinc finger protein, ZFP521, also regulate adipogenesis, in this case by regulating the expression of ZFP423 (Kang et al., 2012). In fact, recent network analysis revealed an entire network of zinc finger proteins, including ZNF264, ZNF490, ZNF587, and ZNF714, which are together expressed in preadipocytes and have a putative role in adipogenesis (Ramirez et al., 2020). Together, these studies implicate a complicated network of zinc finger proteins with non-redundant functionality in the regulation of adipocyte gene expression.

As it relates to the function of ZFP407 in adipocytes, the loss of ZFP407 had a striking effect on adipose tissue morphology, particularly in subcutaneous fat given that the Cre-mediated knockout efficiency appeared significantly higher in that tissue. In this depot, ZFP407 deficiency in adipocytes led to a significant loss of tissue mass and a near complete loss of adipocytes within the remaining fat depot. However, it is not clear whether the depots specific effects observed in AZKO mice are due to depot-specific functions of ZFP407 or whether it is due to technical issues related to the Adiponectin-Cre strain used or the floxed allele of *Zfp407*. Of note, even in the epididymal adipose tissue depots, where little to no reduction in ZFP407 was detected, there were reductions in adipose depot size suggesting that the adipocytes in that depot in which ZFP407 was deleted were not viable. This is consistent with the similar effects on differentiation and gene expression observed in SVF isolated from both subcutaneous and gonadal white adipose tissue depots, suggesting a conserved role for ZFP407 in both of these adipose depots. Nonetheless, the relatively lower ZFP407 expression levels in gonadal fat pads may be associated with depot-specific function as well that will require further experiments to disentangle from the depot specific differences in Cre-mediated deletion efficiency. These allele specific effects on recombination efficacy in different tissues have

been well documented for other Cre driver strains, including the aP2-CreBI strain of mice (Abel et al., 2001). For example, a floxed *Tfam* allele that was crossed with aP2-CreBI mice resulted in a >50% reduction of *Tfam* mRNA in subcutaneous adipocytes, but no decrease in gonadal adipocytes (Lee et al., 2013). In contrast, recombination of a floxed allele of *Shox2* using the same aP2-CreBI strain was equally efficacious in both subcutaneous and gonadal adipose tissue (Lee et al., 2013).

Although the embryonic lethality associated with global ZFP407 deficiency suggests functions beyond the regulation of PPARγ, the lipodystrophic phenotype resulting from adipocyte-specific loss of ZFP407 is largely consistent with a key role of ZFP407 in the regulation of PPARγ signaling as has been previously shown in cultured adipocytes (Buchner et al., 2015). In addition to providing a better understanding of the *in vivo* molecular function of a pathway that is essential for adipogenesis and adipocyte function, PPARγ is also the primary molecular target of the class of drugs known as thiazolidinediones, which includes pioglitazone – one of the most potent FDA-approved insulin sensitizing molecules. This suggests that ZFP407 may also represent a viable therapeutic target for improving insulin sensitivity in type 2 diabetic or pre-diabetic individuals. Given the adverse clinical features associated with thiazolidinedione treatment (Nanjan et al., 2018), it remains possible that treatments targeted to modifiers and co-factors of the PPARγ pathway may improve the balance between therapeutic efficacy and patient safety.

Interestingly, the residual surviving adipocytes that were left in the inguinal depots of AZKO mice were increased in size relative to control mice. One potential mechanism for this hypertrophy may be associated with the overall decrease in fat mass, as inguinal and brown adipose tissues of AZKO mice cumulatively accumulated less lipid while individual cells accumulated more or larger lipid droplets. It's noteworthy

that ZFP407 transgenic overexpressing mice display an increase in plasma β-hydroxybutyrate, which most likely represents increased adipose lipolysis (Charrier et al., 2016). Therefore, we hypothesize that reduced lipolysis due to ZFP407 deficiency could also contribute to the formation of supersized lipid droplets. Since hypertrophy could limit the adipocytes to further expand, the inability to efficiently store lipid in adipocytes of lipodystrophic mice is associated with metabolic dysfunction (Unger and Scherer, 2010; Virtue and Vidal-Puig, 2010). In humans, hypertrophy associates with dyslipidemia, inflammation, and impaired glucose homeostasis (Hoffstedt et al., 2010; Kloting et al., 2010), with hypertrophic adipocytes demonstrating a reduced ability for insulin-stimulated glucose uptake in a cell-autonomous manner (Kim et al., 2015).

Previous studies had shown that ZFP407 is a key factor in regulating insulin-stimulated glucose uptake in 3T3-L1 adipocytes and PPARγ target gene expression (Buchner et al., 2015). These studies were further supported by transgenic mouse ZFP407 overexpression studies similarly demonstrating the positive regulation of PPARγ target genes, including *Glut4*, in skeletal muscle (Charrier et al., 2016). The current studies build upon these findings to reveal an essential role of ZFP407 in adipose tissue formation and organismal insulin sensitivity *in vivo*, therefore providing important insights into the physiological function of ZFP407 and new aspects of gene regulation in adipocytes. Further work is still required to better understanding the molecular mechanisms of ZFP407 in the regulation of PPARγ signaling and its other molecular functions. Given the striking effects on adipocytes caused by ZFP407 deficiency, the molecular insights gained from these studies may lead to new therapeutic strategies for treating human obesity and type 2 diabetes.

Funding

CRediT authorship contribution statement

Alyssa Charrier: Investigation, Writing - original draft, Writing - review & editing, Conceptualization, Data curation, Formal analysis, Funding acquisition. **Xuan Xu:** Investigation, Writing - original draft, Writing - review & editing, Data curation, Formal analysis. **Bo-Jhih Guan:** Investigation, Writing - review & editing. **Justine Ngo:** Investigation, Writing - review & editing. **Anthony Wynshaw-Boris:** Resources, Supervision, Writing - review & editing. **Maria Hatzoglou:** Resources, Supervision, Writing - review & editing. **David A. Buchner:** Resources, Supervision, Writing - original draft, Writing - review & editing, Funding acquisition, Conceptualization.

Declaration of competing interest

The authors declare no conflict of interest.

Acknowledgements

Appendix A. Supplementary data

Supplementary data to this article can be found online at https://doi.org/10.1016/j.mce.2020.111109.

References

Abel, E.D., Peroni, O., Kim, J.K., Kim, Y.B., Boss, O., Hadro, E., Minnemann, T., Shulman, G.I., Kahn, B.B., 2001. Adipose-selective targeting of the GLUT4 gene impairs insulin action in muscle and liver. Nature 409, 729–733. https://doi.org/10.1038/35055575.

Agarwal, A.K., Garg, A., 2002. A novel heterozygous mutation in peroxisome proliferator-activated receptor-gamma gene in a patient with familial partial lipodystrophy. J. Clin. Endocrinol. Metab. 87, 408–411. https://doi.org/10.1210/jcem.87.1.8290.

Barak, Y., Nelson, M.C., Ong, E.S., Jones, Y.Z., Ruiz-Lozano, P., Chien, K.R., Koder, A., Evans, R.M., 1999. PPAR gamma is required for placental, cardiac, and adipose tissue development. Mol. Cell. 4, 585–595. https://doi.org/10.1016/s1097-2765(00)80209-9.

Barroso, I., Gurnell, M., Crowley, V.E., Agostini, M., Schwabe, J.W., Soos, M.A., Maslen, G.L., Williams, T.D., Lewis, H., Schafer, A.J., Chatterjee, V.K., O'Rahilly, S., 1999. Dominant negative mutations in human PPARgamma associated with severe insulin resistance, diabetes mellitus and hypertension. Nature 402, 880–883. https://doi.org/10.1038/47254.

Brayer, K.J., Kulshreshtha, S., Segal, D.J., 2008. The protein-binding potential of C2H2 zinc finger domains. Cell Biochem. Biophys. 51, 9–19. https://doi.org/10.1007/s12013-008-9007-6.

Bryan, A.F., Wang, J., Howard, G.C., Guarnaccia, A.D., Woodley, C.M., Aho, E.R., Rellinger, E.J., Matlock, B.K., Flaherty, D.K., Lorey, S.L., Chung, D.H., Fesik, S.W., Liu, Q., Weissmiller, A.M., Tansey, W.P., 2020. WDR5 is a conserved regulator of protein synthesis gene expression. Nucleic Acids Res. 48, 2924–2941. https://doi.org/10.1093/nar/gkaa051.

Buchner, D.A., Charrier, A., Srinivasan, E., Wang, L., Paulsen, M.T., Ljungman, M., Bridges, D., Saltiel, A.R., 2015. Zinc finger protein 407 (ZFP407) regulates insulin-stimulated glucose uptake and glucose transporter 4 (Glut4) mRNA. J. Biol. Chem. 290, 6376–6386. https://doi.org/10.1074/jbc.M114.623736.

Charrier, A., Wang, L., Stephenson, E.J., Ghanta, S.V., Ko, C.W., Croniger, C.M., Bridges, D., Buchner, D.A., 2016. Zinc finger protein 407 overexpression upregulates PPAR target gene expression and improves glucose homeostasis in mice. Am. J. Physiol. Endocrinol. Metab. 311, E869–E880. https://doi.org/10.1152/ajpendo.00234.2016.

Chiang, S.H., Chang, L., Saltiel, A.R., 2006. TC10 and insulin-stimulated glucose transport. Methods Enzymol. 406, 701–714. https://doi.org/10.1016/S0076-6879(06)06055-1.

Cortes, V.A., Fernandez-Galilea, M., 2015. Lipodystrophies: adipose tissue disorders with severe metabolic implications. J. Physiol. Biochem. 71, 471–478. https://doi.org/10.1007/s13105-015-0404-1.

Duan, S.Z., Ivashchenko, C.Y., Whitesall, S.E., D'Alecy, L.G., Duquaine, D.C., Brosius 3rd, F.C., Gonzalez, F.J., Vinson, C., Pierre, M.A., Milstone, D.S., Mortensen, R.M., 2007. Hypotension, lipodystrophy, and insulin resistance in generalized PPARgamma-deficient mice rescued from embryonic lethality. J. Clin. Invest. 117, 812–822. https://doi.org/10.1172/JCI28859.

Eguchi, J., Wang, X., Yu, S., Kershaw, E.E., Chiu, P.C., Dushay, J., Estall, J.L., Klein, U., Maratos-Flier, E., Rosen, E.D., 2011. Transcriptional control of adipose lipid handling by IRF4. Cell Metabol. 13, 249–259. https://doi.org/10.1016/j.cmet.2011.02.005.

Farley, F.W., Soriano, P., Steffen, L.S., Dymecki, S.M., 2000. Widespread recombinase expression using FLPeR (flipper) mice. Genesis 28, 106–110. https://www.ncbi.nlm.nih.gov/pubmed/11105051.

Fiorenza, C.G., Chou, S.H., Mantzoros, C.S., 2011. Lipodystrophy: pathophysiology and advances in treatment. Nat. Rev. Endocrinol. 7, 137–150. https://doi.org/10.1038/nrendo.2010.199.

Friedel, R.H., Seisenberger, C., Kaloff, C., Wurst, W., 2007. EUCOMM–the European conditional mouse mutagenesis program. Briefings Funct. Genomics Proteomics 6, 180–185. https://doi.org/10.1093/bfgp/elm022.

Guan, B.J., van Hoef, V., Jobava, R., Elroy-Stein, O., Valasek, L.S., Cargnello, M., Gao, X.H., Krokowski, D., Merrick, W.C., Kimball, S.R., Komar, A.A., Koromilas, A.E., Wynshaw-Boris, A., Topisirovic, I., Larsson, O., Hatzoglou, M., 2017. A unique ISR program determines cellular responses to chronic stress. Mol. Cell. 68, 885–900. https://doi.org/10.1016/j.molcel.2017.11.007 e6.

Guarnaccia, A.D., Tansey, W.P., 2018. Moonlighting with WDR5: a cellular multitasker. J. Clin. Med. 7 https://doi.org/10.3390/jcm7020021.

Gupta, R.K., Arany, Z., Seale, P., Mepani, R.J., Ye, L., Conroe, H.M., Roby, Y.A., Kulaga, H., Reed, R.R., Spiegelman, B.M., 2010. Transcriptional control of preadipocyte determination by Zfp423. Nature 464, 619–623. https://doi.org/10.1038/nature08816.

Hata, A., Seoane, J., Lagna, G., Montalvo, E., Hemmati-Brivanlou, A., Massague, J., 2000. OAZ uses distinct DNA- and protein-binding zinc fingers in separate BMP-Smad and Olf signaling pathways. Cell 100, 229–240. https://doi.org/10.1016/s0092-8674(00)81561-5.

He, W., Barak, Y., Hevener, A., Olson, P., Liao, D., Le, J., Nelson, M., Ong, E., Olefsky, J.M., Evans, R.M., 2003. Adipose-specific peroxisome proliferator-activated receptor gamma knockout causes insulin resistance in fat and liver but not in muscle. Proc. Natl. Acad. Sci. U. S. A. 100, 15712–15717. https://doi.org/10.1073/pnas.2536828100.

Hegele, R.A., Cao, H., Frankowski, C., Mathews, S.T., Leff, T., 2002. PPARG F388L, a transactivation-deficient mutant, in familial partial lipodystrophy. Diabetes 51, 3586–3590. https://doi.org/10.2337/diabetes.51.12.3586.

Hoffstedt, J., Arner, E., Wahrenberg, H., Andersson, D.P., Qvisth, V., Lofgren, P., Ryden, M., Thorne, A., Wiren, M., Palmer, M., Thorell, A., Toft, E., Arner, P., 2010.

Regional impact of adipose tissue morphology on the metabolic profile in morbid obesity. Diabetologia 53, 2496–2503. https://doi.org/10.1007/s00125-010-1889-3.

Hu, E., Tontonoz, P., Spiegelman, B.M., 1995. Transdifferentiation of myoblasts by the adipogenic transcription factors PPAR gamma and C/EBP alpha. Proc. Natl. Acad. Sci. U. S. A. 92, 9856–9860. https://doi.org/10.1073/pnas.92.21.9856.

Kang, S., Akerblad, P., Kiviranta, R., Gupta, R.K., Kajimura, S., Griffin, M.J., Min, J., Baron, R., Rosen, E.D., 2012. Regulation of early adipose commitment by Zfp521. PLoS Biol. 10, e1001433 https://doi.org/10.1371/journal.pbio.1001433.

Kersten, S., Desvergne, B., Wahli, W., 2000. Roles of PPARs in health and disease. Nature 405, 421–424. https://doi.org/10.1038/35013000.

Kim, J.I., Huh, J.Y., Sohn, J.H., Choe, S.S., Lee, Y.S., Lim, C.Y., Jo, A., Park, S.B., Han, W., Kim, J.B., 2015. Lipid-overloaded enlarged adipocytes provoke insulin resistance independent of inflammation. Mol. Cell Biol. 35, 1686–1699. https://doi.org/10.1128/MCB.01321-14.

Kloting, N., Fasshauer, M., Dietrich, A., Kovacs, P., Schon, M.R., Kern, M., Stumvoll, M., Bluher, M., 2010. Insulin-sensitive obesity. Am. J. Physiol. Endocrinol. Metab. 299, E506–E515. https://doi.org/10.1152/ajpendo.00586.2009.

Lee, K.Y., Russell, S.J., Ussar, S., Boucher, J., Vernochet, C., Mori, M.A., Smyth, G., Rourk, M., Cederquist, C., Rosen, E.D., Kahn, B.B., Kahn, C.R., 2013. Lessons on conditional gene targeting in mouse adipose tissue. Diabetes 62, 864–874. https://doi.org/10.2337/db12-1089.

Mann, J.P., Savage, D.B., 2019. What lipodystrophies teach us about the metabolic syndrome. J. Clin. Invest. 130, 4009–4021. https://doi.org/10.1172/JCI129190.

Melvin, A., O'Rahilly, S., Savage, D.B., 2018. Genetic syndromes of severe insulin resistance. Curr. Opin. Genet. Dev. 50, 60–67. https://doi.org/10.1016/j.gde.2018.02.002.

Mullican, S.E., Tomaru, T., Gaddis, C.A., Peed, L.C., Sundaram, A., Lazar, M.A., 2013. A novel adipose-specific gene deletion model demonstrates potential pitfalls of existing methods. Mol. Endocrinol. 27, 127–134. https://doi.org/10.1210/me.2012-1267.

Nanjan, M.J., Mohammed, M., Prashantha Kumar, B.R., Chandrasekar, M.J.N., 2018. Thiazolidinediones as antidiabetic agents: a critical review. Bioorg. Chem. 77, 548–567. https://doi.org/10.1016/j.bioorg.2018.02.009.

Ramirez, A.K., Dankel, S.N., Rastegarpanah, B., Cai, W., Xue, R., Crovella, M., Tseng, Y. H., Kahn, C.R., Kasif, S., 2020. Single-cell transcriptional networks in differentiating preadipocytes suggest drivers associated with tissue heterogeneity. Nat. Commun. 11, 2117. https://doi.org/10.1038/s41467-020-16019-9.

Roy, D., Farabaugh, K.T., Wu, J., Charrier, A., Smas, C., Hatzoglou, M., Thirumurugan, K., Buchner, D.A., 2017. Coordinated transcriptional control of adipocyte triglyceride lipase (Atgl) by transcription factors Sp1 and peroxisome proliferator-activated receptor gamma (PPARgamma) during adipocyte differentiation. J. Biol. Chem. 292, 14827–14835. https://doi.org/10.1074/jbc.M117.783043.

Sakaguchi, M., Fujisaka, S., Cai, W., Winnay, J.N., Konishi, M., O'Neill, B.T., Li, M., Garcia-Martin, R., Takahashi, H., Hu, J., Kulkarni, R.N., Kahn, C.R., 2017. Adipocyte dynamics and reversible metabolic syndrome in mice with an inducible adipocyte-specific deletion of the insulin receptor. Cell Metabol. 25, 448–462. https://doi.org/10.1016/j.cmet.2016.12.008.

Savage, D.B., Tan, G.D., Acerini, C.L., Jebb, S.A., Agostini, M., Gurnell, M., Williams, R. L., Umpleby, A.M., Thomas, E.L., Bell, J.D., Dixon, A.K., Dunne, F., Boiani, R., Cinti, S., Vidal-Puig, A., Karpe, F., Chatterjee, V.K., O'Rahilly, S., 2003. Human metabolic syndrome resulting from dominant-negative mutations in the nuclear receptor peroxisome proliferator-activated receptor-gamma. Diabetes 52, 910–917. https://doi.org/10.2337/diabetes.52.4.910.

Schnutgen, F., De-Zolt, S., Van Sloun, P., Hollatz, M., Floss, T., Hansen, J., Altschmied, J., Seisenberger, C., Ghyselinck, N.B., Ruiz, P., Chambon, P., Wurst, W., von Melchner, H., 2005. Genomewide production of multipurpose alleles for the functional analysis of the mouse genome. Proc. Natl. Acad. Sci. U. S. A. 102, 7221–7226. https://doi.org/10.1073/pnas.0502273102.

Shao, M., Hepler, C., Vishvanath, L., MacPherson, K.A., Busbuso, N.C., Gupta, R.K., 2017. Fetal development of subcutaneous white adipose tissue is dependent on Zfp423. Mol Metab 6, 111–124. https://doi.org/10.1016/j.molmet.2016.11.009.

Tan, X., Chen, S., Wu, J., Lin, J., Pan, C., Ying, X., Pan, Z., Qiu, L., Liu, R., Geng, R., Huang, W., 2017. PI3K/AKT-mediated upregulation of WDR5 promotes colorectal cancer metastasis by directly targeting ZNF407. Cell Death Dis. 8, e2686 https://doi.org/10.1038/cddis.2017.111.

Tontonoz, P., Hu, E., Spiegelman, B.M., 1994. Stimulation of adipogenesis in fibroblasts by PPAR gamma 2, a lipid-activated transcription factor. Cell 79, 1147–1156. https://doi.org/10.1016/0092-8674(94)90006-x.

Tontonoz, P., Spiegelman, B.M., 2008. Fat and beyond: the diverse biology of PPARgamma. Annu. Rev. Biochem. 77, 289–312. https://doi.org/10.1146/annurev.biochem.77.061307.091829.

Tsai, R.Y., Reed, R.R., 1997. Cloning and functional characterization of Roaz, a zinc finger protein that interacts with O/E-1 to regulate gene expression: implications for olfactory neuronal development. J. Neurosci. 17, 4159–4169. https://www.ncbi.nlm.nih.gov/pubmed/9151733.

Tsai, R.Y., Reed, R.R., 1998. Identification of DNA recognition sequences and protein interaction domains of the multiple-Zn-finger protein Roaz. Mol. Cell Biol. 18, 6447–6456. https://doi.org/10.1128/mcb.18.11.6447.

Unger, R.H., Scherer, P.E., 2010. Gluttony, sloth and the metabolic syndrome: a roadmap to lipotoxicity. Trends Endocrinol. Metabol. 21, 345–352. https://doi.org/10.1016/j.tem.2010.01.009.

Virtue, S., Vidal-Puig, A., 2010. Adipose tissue expandability, lipotoxicity and the Metabolic Syndrome–an allostatic perspective. Biochim. Biophys. Acta 1801, 338–349. https://doi.org/10.1016/j.bbalip.2009.12.006.

Visser, M.E., Kropman, E., Kranendonk, M.E., Koppen, A., Hamers, N., Stroes, E.S., Kalkhoven, E., Monajemi, H., 2011. Characterisation of non-obese diabetic patients with marked insulin resistance identifies a novel familial partial lipodystrophy-associated PPARgamma mutation (Y151C). Diabetologia 54, 1639–1644. https://doi.org/10.1007/s00125-011-2142-4.

Wang, F., Mullican, S.E., DiSpirito, J.R., Peed, L.C., Lazar, M.A., 2013. Lipoatrophy and severe metabolic disturbance in mice with fat-specific deletion of PPARgamma. Proc. Natl. Acad. Sci. U. S. A. 110, 18656–18661. https://doi.org/10.1073/pnas.1314863110.